5028 *Biochemistry* **2010,** *49,* 5028–5034
DOI: 10.1021/bi1005078

BIOCHEMISTRY
including biophysical chemistry & molecular biology
Article

Spectroscopic Studies of Ligand and Substrate Binding to Human Indoleamine 2,3-Dioxygenase

Changyuan Lu, Yu Lin, and Syun-Ru Yeh*

Department of Physiology and Biophysics, Albert Einstein College of Medicine, 1300 Morris Park Avenue, Bronx, New York 10461

Received April 3, 2010; Revised Manuscript Received May 13, 2010

ABSTRACT: Human indoleamine 2,3-dioxygenase (hIDO) is an intracellular heme-containing enzyme, which catalyzes the initial and rate-determining step of L-tryptophan (L-Trp) metabolism via the kynurenine pathway in nonhepatic tissues. Steady-state kinetic data showed that hIDO exhibits substrate inhibition behavior, implying the existence of a second substrate binding site in the enzyme, although so far there is no direct evidence supporting it. The kinetic data also revealed that the K_m of L-Trp (15 μM) is ~27-fold lower than the K_d of L-Trp (0.4 mM) for the ligand-free ferrous enzyme, suggesting that O_2 binding proceeds L-Trp binding during the catalytic cycle. With cyanide as a structural probe, we have investigated the thermodynamic and kinetic parameters associated with ligand and substrate binding to hIDO. Equilibrium titration studies show that the cyanide adduct is capable of binding two L-Trp molecules, with K_d values of 18 μM and 26 mM. The data offer the first direct evidence of the second substrate binding site in hIDO. Kinetic studies demonstrate that prebinding of L-Trp to the enzyme retards cyanide binding by ~13-fold, while prebinding of cyanide to the enzyme facilitates L-Trp binding by ~22-fold. The data support the view that during the active turnover of the enzyme it is kinetically more favored to bind O_2 prior to L-Trp.

L-Tryptophan (L-Trp)[1] is the scarcest essential amino acid in mammals. Most of our dietary Trp is metabolized in the liver along the kynurenine pathway, which ultimately leads to the biosynthesis of NAD (*1*−*4*). The conversion of L-Trp to *N*-formylkynurenine (NFK), the initial and rate-determining step of the kynurenine pathway, is catalyzed by a hepatic heme-based dioxygenase, tryptophan 2,3-dioxygenase (TDO), via insertion of both atoms of dioxygen into the C_2=C_3 bond of the indole moiety of L-Trp (Scheme 1). In addition to TDO, a second heme-based dioxygenase, indoleamine 2,3-dioxygenase (IDO), discovered by Hayaishi et al. in 1967 (*5*), catalyzes the same oxidative ring cleavage reaction of L-Trp to NFK. In contrast to the hepatic TDO, IDO is ubiquitously distributed in all tissues other than liver. In addition, instead of regulating homeostatic serum Trp concentrations like TDO, IDO can be induced by IFN-γ and closely linked to immunomodulation by regulating T cell activity via controlling L-Trp catabolism (*6*, *7*). Recently, IDO has attracted a great deal of attention because of its potential as a therapeutic target for cancer and neurological disorders (*8*, *9*).

IDO is present only in mammals. The overall structure of the human isoform (hIDO), resolved by Sugimoto et al. in 2006 (*10*), displays two α-helical domains sandwiching the prosthetic heme group. The structure of the large domain of IDO is highly similar with that of TDO, suggesting that the two dioxygenases carry out the dioxygen chemistry with a similar mechanism. Consistently, recent resonance Raman studies combined with MD and QM/MM simulations reveal that the dioxygenase reactions carried out by IDO and TDO follow a common mechanism, by which the two atoms of the heme-bound dioxygen are inserted into the substrate one at a time via a ferryl intermediate (*11*). Despite the structural and functional similarities, IDO exhibits several unique properties distinguishing itself from TDO. (i) IDO forms relatively stable dioxygen adducts regardless of Trp (*12*), whereas the dioxygen complex of TDO is stable only in the presence of Trp (*13*). (ii) The ternary complex of IDO can be readily oxidized by releasing O_2 as superoxide, while that of TDO is much less susceptible to autoxidation (*14*). (iii) The binding of L-Trp in IDO retards CO binding, while that in TDO accelerates it (*12*, *13*). (iv) The ferric derivative of IDO reacts with superoxide to form the active oxy complex, while that of TDO does not bind superoxide (*14*, *15*).

As illustrated in Scheme 2, it is generally believed that during the active catalytic cycle of hIDO (indicated by the black arrows), the ferrous enzyme first binds L-Trp, followed by O_2 binding, to generate the ternary complex, which turns over to produce the product, NFK, leaving the enzyme in the catalytically competent ferrous state. During the reaction, a small amount of enzyme may leak out of the active cycle via autoxidation to the inactive ferric state, which can return to the active cycle only by accepting an electron or by binding a superoxide (see the gray arrows). The sequential binding of Trp and O_2 was first proposed on the basis of the observation that the apparent Michaelis−Menten constant (K_m) of L-Trp (13 μM) for the rabbit isoform of the enzyme (rIDO) matches the equilibrium dissociation constant, K_d (L-Trp), of the ligand-free ferrous enzyme (*14*, *16*). However, recent data show that the K_m of the human isoform (~15 μM) is ~40-fold lower than the K_d (L-Trp) of the ligand-free enzyme (0.53 mM) (*10*, *17*), implying that in hIDO, O_2 binding proceeds L-Trp binding as illustrated by the red arrows in Scheme 2.

*To whom correspondence should be addressed: Department of Physiology and Biophysics, Albert Einstein College of Medicine, Bronx, NY 10461. Telephone: (718) 430-4234. Fax: (718) 430-4230. E-mail: syun-ru.yeh@einstein.yu.edu.

[1]Abbreviations: IDO, indoleamine 2,3-dioxygenase; TDO, tryptophan 2,3-dioxygenase; hIDO, human indoleamine 2,3-dioxygenase; rIDO, rabbit indoleamine 2,3-dioxygenase; IFN-γ, interferon-γ; NFK, *N*-formylkynurenine; L-Trp, L-tryptophan.

 Published on Web 05/17/2010

Scheme 1: Dioxygenation Reaction of Tryptophan Catalyzed by IDO and TDO

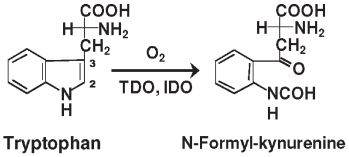

Scheme 2: Catalytic Cycle of Human Indoleamine 2,3-Dioxygenase

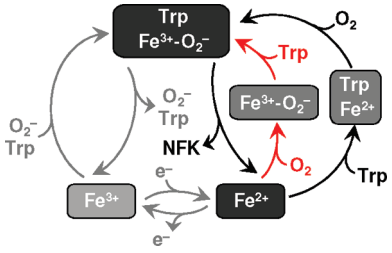

Although the structural origin of the differences observed in hIDO with respect to rIDO remains unknown, the data suggest that the kinetic and thermodynamic properties associated with O_2 and Trp binding are isoform-specific and evolutionarily optimized.

It has been recognized several decades ago that the steady-state activity of rIDO follows Michaelis−Menten behavior at <0.2 mM L-Trp, yet a further increase in the L-Trp concentration leads to a decrease in the activity (*5*, *16*). It was initially believed that, at high concentrations of L-Trp, the substrate binds to the ferric enzyme, thereby inhibiting the turnover of the enzyme by retarding its reduction to the active ferrous state (*16*). However, recent studies suggest that this scenario is not operative in hIDO on the basis of two new observations. (i) L-Trp binding to the ferric enzyme promotes, instead of retards, its reduction (from a thermodynamic point of view) (*18*), and (ii) the K_d (L-Trp) of the ferric enzyme (0.9 mM) is much higher than the self-inhibition constant (K_{si}, 0.17 mM) (*17*). Additional data for hIDO indicate that, at high concentrations, the substrate can bind to an inhibitory substrate binding site in addition to the active site, thereby accounting for the substrate inhibition behavior (*17*). Although recent ligand rebinding studies of CO-bound hIDO at cryogenic temperatures provide kinetic evidence supporting the two substrate binding sites in hIDO (*19*), so far there are no direct experimental data demonstrating the existence of the inhibitory substrate binding site in hIDO.

Recent resonance Raman data of the O_2 adduct of hIDO show that, instead of $Fe^{2+}-O_2$ character, it exhibits $Fe^{3+}-O_2^-$ character (*11*), suggesting that the O_2 adduct can be mimicked by the $Fe^{3+}-CN^-$ complex. In this work, we sought to use cyanide as a structural probe to investigate the thermodynamic and kinetic properties associated with substrate and ligand binding to hIDO. Our data provide the first direct evidence supporting the second substrate binding site in hIDO; they also revealed that prebinding of L-Trp to the enzyme retards the subsequent binding of cyanide, while prebinding of cyanide facilitates the subsequent binding of L-Trp, both observations being consistent with the view that Trp binding is substantially promoted by binding of the small dioxygen ligand.

MATERIALS AND METHODS

Materials. L-Tryptophan (L-Trp) and potassium cyanide (KCN) were purchased from Aldrich. All chemicals used were of analytical reagent grade without further purification. All solutions were prepared with deionized (Millipore) water. Columns and media for protein purification were from Amersham Pharmacia Biotech.

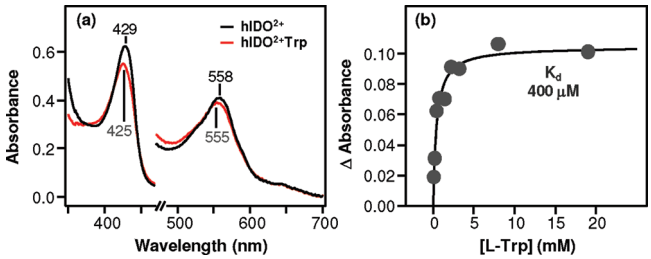

FIGURE 1: Absorption spectra of ferrous hIDO (a) and equilibrium titration curve of ferrous hIDO with L-Trp (b). The absorption spectra in panel a were recorded in the absence (black curve) or presence (red curve) of 20 mM L-Trp. The ΔA values in panel b were measured at 428 nm. All the data were obtained with 5.5 μM hIDO in 100 mM Tris buffer (pH 7.4) at room temperature.

Protein Expression and Purification. The recombinant hIDO protein was prepared as described previously (*20*). The protein concentration was estimated by using the Soret absorption at 404 nm with an extinction coefficient of 172 mM^{-1} cm^{-1} for the ferric form (*18*). The catalytic activity of hIDO was confirmed by monitoring the increase in optical absorption at 321 nm, indicative of product (*N*-formylkynurenine) formation, with an extinction coefficient of 3.75 mM^{-1} cm^{-1} (*13*, *17*). The protein was stored at −80 °C until it was used. We prepared the ferrous ligand-free sample by first flushing the sample with Ar gas and then reducing it with a 5-fold molar excess of sodium dithionite. Unless otherwise indicated, the hIDO samples were buffered with 100 mM Tris-HCl and 50 μM EDTA (pH 7.4).

Optical Absorption Measurements. The optical absorption spectra were recorded by using a Shimadzu spectrophotometer (Shimadzu Co., Kyoto, Japan). All spectra were recorded at room temperature (~25 °C). The protein concentrations were ~1−10 μM. The equilibrium ligand and substrate binding data were fitted with eq 1 by using Origin version 6.1 (Microcal, Inc., Northampton, MA) (*21*).

$$\Delta A = \Delta A_{max}\{[hIDO] + [L] + K_d - [([hIDO]+[L]+K_d)^2 - 4[hIDO][L]]^{1/2}\}/(2[hIDO]) \quad (1)$$

where [L] and [hIDO] are the ligand (or substrate) and enzyme concentrations, respectively, K_d is the ligand (or substrate) dissociation constant, and ΔA and ΔA_{max} are the observed and maximum changes in absorbance, respectively.

Stopped-Flow Measurements. The transient kinetics experiments were performed with a π*180 stopped-flow instrument from Applied Photophysics Inc. (Leatherhead, U.K.) (*22*). The progression of the reaction was monitored in optical absorption mode with a photodiode array detector at 20 °C. The data were analyzed using Pro-K software provided by Applied Photophysics. The concentration of L-Trp or cyanide was at least 5-fold higher than that of the protein, so that all the reactions were conducted under pseudo-first-order conditions.

RESULTS AND DISCUSSION

K_d (L-Trp) of Ferrous and Ferric hIDO. The optical absorption spectrum of the substrate-free ferrous hIDO exhibits a Soret maximum at 429 nm (Figure 1a) and a Q-band at 558 nm (as listed in Table 1), characteristics of five-coordinate high-spin

Table 1: Soret Bands and Q-Bands of the Various Derivatives of hIDO

	λ_{Soret} (nm)	λ_{vis} (nm)
Fe^{3+}	404	499, 533, 633
Fe^{3+}−L-Trp	410	540, 576
Fe^{3+}−CN^-	419	541, 570
Fe^{3+}−L-Trp−CN^-	416	541, 570
Fe^{2+}	429	558
Fe^{2+}−L-Trp	425	555

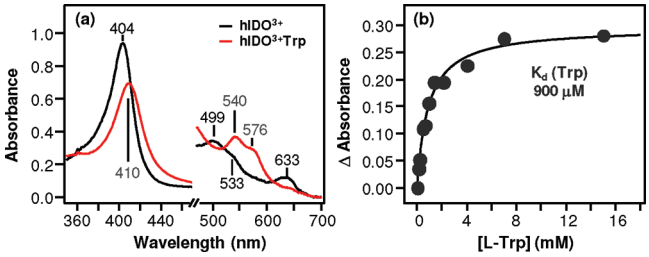

FIGURE 2: Absorption spectra of ferric hIDO (a) and equilibrium titration curve of ferric hIDO with L-Trp (b). The absorption spectra in panel a were recorded in the absence (black curve) or presence (red curve) of 20 mM L-Trp. The ΔA values in panel b were measured at 404 nm. All the data were obtained with 5.5 μM hIDO in 100 mM Tris buffer (pH 7.4) at room temperature.

ferrous heme species. The binding of L-Trp causes the shift of the Soret and Q-bands to 425 and 555 nm, respectively. L-Trp titration studies show a typical hyperbolic behavior (Figure 1b), with a K_d of 0.40 ± 0.07 mM based on curve fitting of the data with a single-binding site model described in eq 1, which is consistent with the reported value (0.53 mM) (*10*). The data confirm that the K_d of L-Trp for the active ferrous enzyme is much higher than the K_m of L-Trp (15 μM) observed during steady-state reactions (*17*), supporting the view that during the catalytic cycle L-Trp binding does not proceed O_2 binding. It is noteworthy that the spectral feature of the L-Trp-bound ferrous hIDO shown in Figure 1a is distinct from that reported by Chauhan et al. (with λ_{max} at 413, 551, and 575 nm) (*23*), as in the latter case the spectrum is likely derived from a mixture of deoxy and O_2-bound enzyme (the latter exhibits λ_{max} at 412, 542, and 576 nm) (*11*).

The optical absorption spectrum of the substrate-free ferric hIDO, on the other hand, exhibits a Soret maximum at 404 nm and Q-bands at 499 and 533 nm (Figure 2a), as well as a charge transfer band at 633 nm, characteristics of a water-bound ferric species. The binding of L-Trp causes the shift of the Soret maximu to 410 nm and Q-bands to 540 and 576 nm, which is accompanied by the disappearance of the charge transfer band, characteristic of a hydroxide-bound ferric species, as revealed by resonance Raman studies (*20*), suggesting substrate-induced deprotonation of the heme-bound water.

In the P450 or NOS class of enzymes (with thiolate as the proximal heme ligand), substrate binding typically results in the displacement of the heme-bound water (*24*, *25*), due to steric hindrance introduced by substrate occupying the distal heme pocket. The substrate binding-induced deprotonation of the heme-bound water in hIDO indicates that the indoleamine or amino group of the L-Trp is located in the proximity of the water, thereby perturbing its pK_a. The enzyme-specific substrate−ligand interactions are plausibly optimized for each of these oxygen-utilizing enzymes to selectively enhance specific functions.

L-Trp titration of the ferric species shows typical hyperbolic behavior with a K_d value of 0.90 ± 0.09 mM (Figure 2b), based on curve fitting of the data with a single-binding site model described in eq 1. The slight decrease in K_d (L-Trp) from 0.9 to 0.4 mM upon reduction is consistent with the observation that substrate binding in hIDO leads to a small increase in its redox potential (~46 mV) (*18*). The substrate-induced redox potential change in hIDO is substantially weaker than those observed in P450 and NOS [157 mV (*14*, *26*) and 84 mV (*27*) for $P450_{cam}$ and iNOS, respectively]. It is generally believed that the substrate binding-induced increase in the redox potential of P450 and NOS plays a critical role in preventing the formation and release of superoxide, which is toxic to cells, under substrate-deficient conditions in vivo. For hIDO, the autoxidation rate of the O_2 complex of hIDO is relatively slow in the absence of substrate; this type of cellular protection mechanism, hence, might not be vital. However, it is noteworthy that, in contrast to P450 and NOS, IDO exhibits a much higher autoxidation rate in the substrate-bound state (*14*) (for reasons yet to be resolved); consequently, an exogenous electron source is required to sustain the multiple turnovers of the enzyme in vitro, despite the fact that the dioxygenase reaction does not consume any electron (Scheme 1).

K_d (L-Trp) of Cyanide-Bound Ferric hIDO. Cyanide binding to the substrate-free ferric enzyme causes the shift of the Soret maximum to 419 nm and Q-bands to 541 and 570 nm (Figure 3a). Titration studies show a high affinity of cyanide for hIDO, with a K_d of 2.4 ± 0.2 μM on the basis of the data fitting with eq 1 (Figure 3b).

The addition of 1 mM L-Trp to the cyanide-bound enzyme leads to the shift of the Soret maximum to 416 nm, as well as a small change in the Q-bands (Figure 3a). The spectral change is consistent with the published resonance Raman data showing that the cyanide-related vibrational modes (including ν_{Fe-CN} and δ_{Fe-C-N} modes) are significantly perturbed by L-Trp binding, implying the proximity of L-Trp to the heme-bound cyanide (*20*). A further increase in the L-Trp concentration to 44 mM surprisingly induces partial recovery of the intensity of the Soret band without affecting its maximum position. To understand the spectral transitions, the cyanide-bound enzyme was titrated with L-Trp. As shown in Figure 3c, two transitions with K_d values of 18 ± 3 μM and 26 ± 8 mM are revealed.

The clear two-step transition shown in Figure 3c provides the first experimental evidence demonstrating the existence of two substrate binding sites in hIDO. The K_d value for the second substrate binding site, 26 mM, is much higher than the substrate inhibition constant (K_{si}), 0.17 mM, observed during the steady-state turnover of the enzyme, indicating that the affinity of L-Trp for the second binding site is sensitive to the redox and/or ligation state of the heme iron. Likewise, the K_d value of the first binding site, 18 μM, is much lower than that of the CO-bound form [0.12 mM (C. Lu et al., results to be published)], as well as those of the ligand-free ferric enzyme (0.9 mM) and ferrous enzyme (0.4 mM). Taken together, the data indicate that the redox-state change and/or ligand binding to the heme iron introduces significant structural perturbations into the protein matrix housing the two substrate binding sites and that the second substrate binding site cannot be observed in the ligand-free ferric and ferrous enzyme (see Figures 1b and 2b).

L-Trp Binding Kinetics. To investigate the structural perturbation introduced by cyanide binding to the heme iron, L-Trp binding to the ligand-free and cyanide-bound hIDO was studied with stopped-flow measurements. As shown in Figure 4a, the kinetic trace at 403 nm obtained from the reaction of the ligand-free enzyme with 0.75 mM L-Trp follows single-exponential

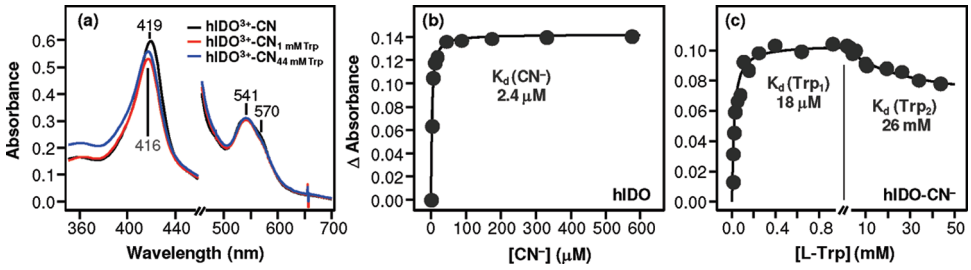

FIGURE 3: Absorption spectra of cyanide-bound ferric hIDO (a) and equilibrium titration curve of the substrate-free ferric hIDO with cyanide (b) or that of the cyanide-bound hIDO with L-Trp (c). The absorption spectra in panel a were recorded in the absence (black curve) or presence of 1 mM L-Trp (red curve) or 44 mM L-Trp (blue curve). The ΔA values in panels b and c were measured at 403 and 423 nm, respectively. The data were obtained with 4.7 μM hIDO (a and c) and 1.5 μM hIDO (b) in 100 mM Tris buffer (pH 7.4) at room temperature. The cyanide concentration used for panels a and c was 1 mM.

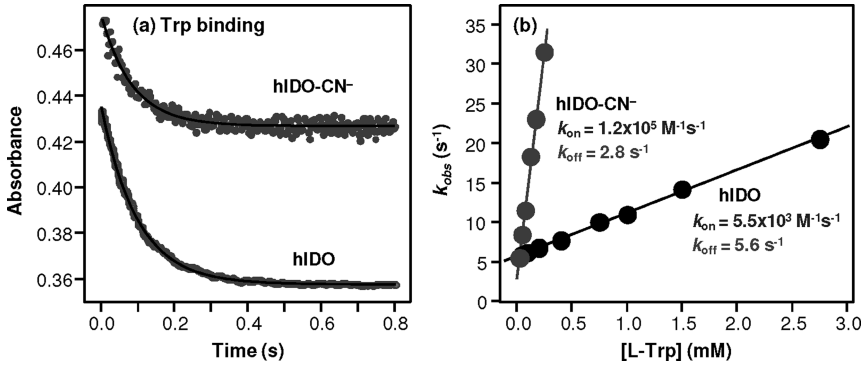

FIGURE 4: L-Trp binding kinetics of cyanide-free and cyanide-bound ferric hIDO (a) and plot of the observed rate constants as a function of L-Trp concentration (b). The kinetic traces of the cyanide-free hIDO (2.5 μM) and cyanide-bound hIDO (4.0 μM) shown in panel a were obtained with 750 μM L-Trp at 403 nm and 75 μM Trp at 421 nm, respectively. The solid lines in panel a are the best-fit curves with single-exponential functions. All the samples were prepared in 100 mM Tris buffer (pH 7.4) at 20 °C, in the presence or absence of 1 mM cyanide.

decay kinetics, with an observed rate constant of 10 s^{-1}. The observed rate constant depends on the L-Trp concentration in a linear fashion (Figure 4b). The bimolecular binding rate constant (k_{on}) obtained from the slope of the best-fit line is (5.5 ± 0.1) × 10^3 M^{-1} s^{-1}, while the dissociation rate constant (k_{off}) obtained from the intercept is 5.6 ± 0.1 s^{-1}. The K_d calculated from the k_{off}/k_{on} (1.0 mM) is consistent with that observed from equilibrium measurements (0.9 mM), confirming the reliability of the kinetic measurements. It is noteworthy that there is a typo in the unit of the previously published k_{on}, 1.55 × 10^4 μM^{-1} s^{-1} (*23*), which should be M^{-1} s^{-1} (Emma Raven, private communication), hence the k_{on} we determined, 5.5 × 10^3 M^{-1} s^{-1}, is similar to the reported value.

In the presence of cyanide, the L-Trp binding kinetics were found to be much faster (Figure 4a,b). L-Trp concentration-dependent data show that the k_{on} and k_{off} determined from the slope and intercept of the best-fit line are (1.2 ± 0.1) × 10^5 M^{-1} s^{-1} and 2.8 ± 0.4 s^{-1}, respectively (Figure 4b). The K_d calculated from the k_{off}/k_{on} (23 μM) again is consistent with that observed from equilibrium measurements (18 μM). It is important to note that the L-Trp concentrations employed here are less than 0.3 mM; hence, only the first Trp binding site is occupied. Kinetic studies conducted with higher L-Trp concentrations revealed that the binding of L-Trp to the second binding site is too fast to be measured with our instrument.

Cyanide Binding Kinetics. To examine how the L-Trp bound in the distal heme pocket perturbs ligand binding kinetics, cyanide binding to the substrate-free and L-Trp-bound enzyme was studied with stopped-flow measurements. As shown in Figure 5a, the kinetic trace at 404 nm obtained from the reaction of the substrate-free enzyme with 87 μM cyanide follows single-exponential decay kinetics, with an observed rate constant of 0.38 s^{-1}. Concentration-dependent studies show that the k_{on} and k_{off} values are (4.1 ± 0.1) × 10^3 M^{-1} s^{-1} and 0.018 ± 0.006 s^{-1}, respectively (Figure 5b). The K_d calculated from the k_{off}/k_{on} (4.4 μM) is consistent with that observed from equilibrium measurements (2.4 μM) and is similar to the published value (3.6 μM) (*23*).

In the presence of L-Trp, the cyanide binding kinetics also follows single-exponential kinetics (Figure 5a). It is important to note that the reaction was conducted in the presence of 25 mM L-Trp to ensure that all the protein molecules are in the L-Trp-bound state during the reaction. With 25 mM L-Trp, ~50% of the molecules are in the two-Trp-bound state at the end of the reaction (considering the fact that the K_d for the second substrate binding site is 26 mM). As such, two parallel reactions illustrated below have to be taken into account (assuming that the ferric ligand-free enzyme comprises only one substrate binding site).

$$IDO^{3+}\cdot(Trp) + CN^- \underset{k_{off}}{\overset{k_{on}}{\rightleftharpoons}} IDO^{3+}-CN^-\cdot(Trp)$$

$$IDO^{3+}\cdot(Trp) + CN^- \underset{k_{off}}{\overset{k_{on}}{\rightleftharpoons}} IDO^{3+}-CN^-\cdot(Trp)$$

$$+ Trp \underset{k_{off}'}{\overset{k_{on}'}{\rightleftharpoons}} IDO^{3+}-CN^-\cdot(Trp)_2$$

As the second reaction is limited in rate by cyanide binding (i.e., $k_{on}[CN^-] \ll k_{on}'[\text{L-Trp}]$), the overall reaction follows single-exponential kinetics with a rate constant of k_{on} as demonstrated in Figure 5a. Concentration-dependent studies show that the k_{on} is (3.2 ± 0.1) × 10^2 M^{-1} s^{-1} while the k_{off} is too slow to be precisely determined (Figure 5b).

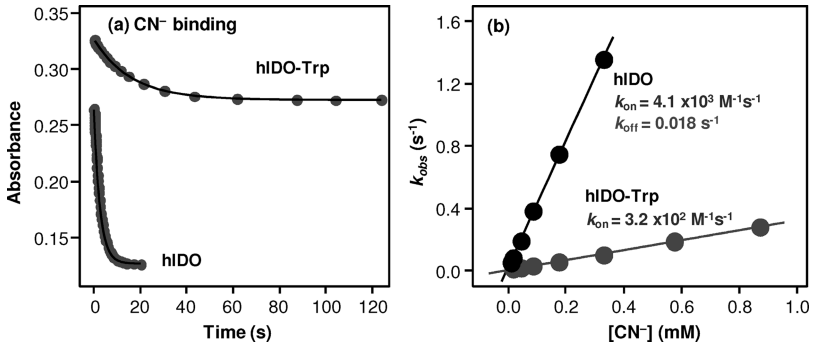

FIGURE 5: Cyanide binding kinetics of substrate-free and L-Trp-bound ferric hIDO (a) and plot of the observed rate constants as a function of cyanide concentration (b). The kinetic traces of the substrate-free hIDO (1.5 μM) and L-Trp-bound hIDO (3.1 μM) shown in panel a were obtained with 87 μM cyanide at 404 and 410 nm, respectively. The solid lines in panel a are the best-fit curves with single-exponential functions. All the samples were prepared in 100 mM Tris buffer (pH 7.4) at 20 °C, in the presence or absence of 25 mM L-Trp.

Table 2: Kinetic and Thermodynamic Parameters Associated with Cyanide or L-Trp Binding Reactions of hIDO, rIDO, and TDO

	hIDO				rIDO	TDO
	k_{on} (M^{-1} s^{-1})	k_{off} (s^{-1})	K_d (μM)[b]	K_d^{eq} (μM)	K_d^{eq} (μM)	K_d^{eq} (μM)
Fe^{2+} + Trp	ND	ND		$(4.0 \pm 0.7) \times 10^2$	13[d]	4.12[g]
Fe^{3+} + Trp	$(5.5 \pm 0.1) \times 10^3$	5.6 ± 0.1	1.0×10^3	$(9.0 \pm 0.9) \times 10^2$	5.8×10^3[d] 3.0×10^4[f]	3.8×10^3[g]
Fe^{3+}−CN^- + Trp	$(1.2 \pm 0.1) \times 10^5$	2.8 ± 0.4	23	18 ± 3	10−20[e] 16[f]	
Fe^{3+} + CN^-	$(4.1 \pm 0.1) \times 10^3$	0.018 ± 0.006	4.4	2.4 ± 0.2	11[f]	
Fe^{3+}−Trp + CN^-	$(3.2 \pm 0.1) \times 10^2$	3.2×10^{-5}[a]	0.1[a]	0.05[a]	0.5[f]	
Fe^{3+}−Trp− CN^- + Trp				$(2.6 \pm 0.8) \times 10^4$		
K_m (μM)	15 ± 2[c]				12[d]	114[g]

[a]Calculated from the thermodynamic cycle illustrated in Figure 6. [b]Calculated from k_{on}/k_{off}. [c]From ref *17*. [d]From ref *16*. [e]From ref *34*. [f]From ref *35*. [g]From ref *33*.

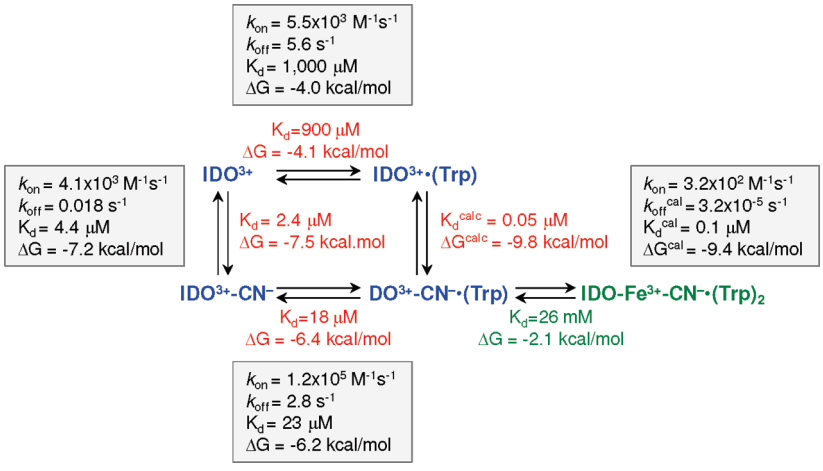

FIGURE 6: Thermodynamic cycle describing the cyanide and L-Trp binding reactions of hIDO. The parameters labeled in red were obtained from equilibrium measurements. The parameters listed in the shaded boxes were obtained from kinetic measurements. The free energy (ΔG) values associated with ligand or substrate binding were calculated from K_d, on the basis of the relationship $\Delta G = RT\ln(K_d)$. The side reaction labeled in green is associated with the binding of L-Trp to the second substrate binding site in the cyanide-bound enzyme.

Implication for the Catalytic Cycle of hIDO. The thermodynamic and kinetic parameters associated with binding of L-Trp and cyanide to hIDO obtained from this work are summarized in Table 2. On the basis of the thermodynamic cycle illustrated in Figure 6, the ΔG for cyanide binding to L-Trp-bound ferric hIDO is calculated to be −9.4 kcal/mol (or −9.8 kcal/mol based on the equilibrium data). The K_d and k_{off} calculated from the ΔG are 0.1 μM and 3.2×10^{-5} s^{-1}, respectively.

Taken together, the data show that prebinding of L-Trp to the enzyme retards cyanide binding and dissociation by 13- and 560-fold, respectively, indicating that L-Trp bound in the distal heme pocket restricts the access of ligand to the heme iron and escape of ligand from the heme iron. The net result is tighter cyanide binding, with a $\Delta\Delta G$ of −2.3 kcal/mol. On the other hand, prebinding of cyanide to the enzyme facilitates L-Trp binding by 22-fold but retards its dissociation by 2-fold, indicating that cyanide binding to the heme iron introduces structural changes to the protein matrix allowing faster access of the substrate to the active site and slower dissociation from it. The net result is tighter substrate binding, with a $\Delta\Delta G$ of −2.3 kcal/mol.

The positive cooperativity between cyanide and L-Trp binding (i.e., cyanide binding increases the binding affinity of L-Trp, and vice versa) highlights the plasticity of the enzyme.

Steady-state kinetic studies show that the K_m of L-Trp for hIDO is 15 μM (*17*), which is 27-fold lower than the K_d(L-Trp) of the ligand-free ferrous enzyme (0.4 mM), while the K_m of O_2 (42 μM) (*17*) is similar to the $K_d(O_2)$ of the substrate-free ferrous enzyme (13 μM) (*23*), suggesting that during multiple turnovers hIDO preferentially binds O_2 prior to L-Trp. The physiological concentrations of L-Trp and O_2 in tissues and plasma are typically in the ranges of 50−100 μM (*28*, *29*) and 50−76 μM (*30*, *31*), respectively. On the basis of the K_d(L-Trp) and $K_d(O_2)$ of the ferrous enzyme (400 and 13 μM, respectively), 50 μM L-Trp forces ~5% enzyme into the substrate-bound form, while 50 μM O_2 leads to >85% O_2-bound enzyme; as such, under physiological conditions, prebinding of O_2 followed by L-Trp binding, as indicated by the red arrows in Scheme 2, is thermodynamically favored. On the other hand, the data present in this work demonstrate that ligand binding-induced structural changes in the enzyme facilitate L-Trp binding by 22-fold, while the L-Trp binding-induced structural transition retards cyanide binding by 13-fold, suggesting that a sequential binding of O_2 and L-Trp is also kinetically favored during the catalytic cycle.

One unique feature of the dioxygenase family of enzymes with respect to other oxygen-utilizing heme proteins, such as P450 and NOS, is the relatively weak substrate affinity in the ferric state. As listed in Table 2, the substrate affinities of ferric hIDO, rIDO, and xcTDO are in the millimolar window, which are much lower than the affinity of ~2 μM observed in P450 and NOS (*16*, *17*, *27*, *32*, *33*). In P450 and NOS, the reduction of the heme iron only slightly perturbs the substrate affinity (*24*, *27*), while that in rIDO and xcTDO leads to an ~500−1000-fold increase in substrate affinity (*16*, *33*). In contrast, reduction of hIDO improves the substrate affinity by only ~2-fold. The low substrate affinity of the ferrous hIDO is presumably important for ensuring that the enzyme binds O_2 prior to substrate binding during multiple turnovers. The physiological importance of this unique property of hIDO remains to be investigated further; nonetheless, the sequential binding of O_2 and L-Trp may be critical for downregulating the hIDO activity at high L-Trp concentrations via the substrate inhibition mechanism (as the inhibitory substrate binding site can be observed only in the ligand-bound state).

CONCLUSIONS

Dioxygen-activating oxygenases can be divided into two groups: (i) monooxygenases (such as P450s), which incorporate one atom of the dioxygen into an organic substrate and reduce the other atom of the dioxygen to water, and (ii) dioxygenases (such as IDO and TDO), which insert both atoms of dioxygen into the substrate. In contrast to the wide spectrum of P450-type enzymes, hIDO and hTDO are the only two heme-based dioxygenases found in humans. The catalytic cycle of P450 has been studied in great detail (*14*, *24*). In general, the substrate binds the enzyme in the ferric state, which leads to the displacement of the heme-bound water. It increases the redox potential of the enzyme and triggers the transfer of the electron from the reductase to the heme iron. The resulting ferrous heme iron binds O_2, leading to the ternary complex, in which the O−O bond is heterolytically cleaved upon accepting an additional electron and a proton. The cleavage reaction generates a key ferryl intermediate, which is capable of inserting a single oxygen into the organic substrates, thereby producing the products. The catalytic cycle of hIDO, on the other hand, is much less clear. Nonetheless, it is generally believed that the dioxygenase reaction is initiated in the ferrous state. Our data reported here suggest that the ferrous enzyme first binds O_2, followed by L-Trp binding, to generate the ternary complex. The heme-bound O_2 in the ternary complex is then inserted into the C_2=C_3 bond of the indole ring of the substrate, leading to a ferryl intermediate and a Trp epoxide (via an alkylperoxo transition state), which subsequently recombine to generate the product (*11*). We postulate that the sequential binding of O_2 and substrate during the catalytic cycle of hIDO is important for downregulating the activity of the enzyme at high L-Trp concentrations via its binding to the inhibitory substrate binding site, which can be observed only in the ligand-bound state.

ACKNOWLEDGMENT

We thank Dr. Denis L. Rousseau for valuable discussions.

REFERENCES

1. Kotake, Y., and Masayama, T. (1936) Uber den mechanismus der kynurenin-bildung aus tryptophan. *Z. Physiol. Chem. 243*, 237–244.
2. Greengard, O., and Feigelsonp, P. (1962) The purification and properties of liver tryptophan pyrrolase. *J. Biol. Chem. 237*, 1903–1907.
3. Schutz, G., Chow, E., and Feigelson, P. (1972) Regulatory properties of hepatic tryptophan oxygenase. *J. Biol. Chem. 247*, 5333–5337.
4. Ren, S., and Correia, M. A. (2000) Heme: A regulator of rat hepatic tryptophan 2,3-dioxygenase? *Arch. Biochem. Biophys. 377*, 195–203.
5. Yamamoto, S., and Hayaishi, O. (1967) Tryptophan pyrrolase of rabbit intestine. D- and L-tryptophan-cleaving enzyme or enzymes. *J. Biol. Chem. 242*, 5260–5266.
6. Muller, A. J., and Prendergast, G. C. (2007) Indoleamine 2,3-dioxygenase in immune suppression and cancer. *Curr. Cancer Drug Targets 7*, 31–40.
7. Katz, J. B., Muller, A. J., and Prendergast, G. C. (2008) Indoleamine 2,3-dioxygenase in T-cell tolerance and tumoral immune escape. *Immunol. Rev. 222*, 206–221.
8. Uyttenhove, C., Pilotte, L., Theate, I., Stroobant, V., Colau, D., Parmentier, N., Boon, T., and Van den Eynde, B. J. (2003) Evidence for a tumoral immune resistance mechanism based on tryptophan degradation by indoleamine 2,3-dioxygenase. *Nat. Med. 9*, 1269–1274.
9. Muller, A. J., DuHadaway, J. B., Donover, P. S., Sutanto-Ward, E., and Prendergast, G. C. (2005) Inhibition of indoleamine 2,3-dioxygenase, an immunoregulatory target of the cancer suppression gene Bin1, potentiates cancer chemotherapy. *Nat. Med. 11*, 312–319.
10. Sugimoto, H., Oda, S., Otsuki, T., Hino, T., Yoshida, T., and Shiro, Y. (2006) Crystal structure of human indoleamine 2,3-dioxygenase: Catalytic mechanism of O_2 incorporation by a heme-containing dioxygenase. *Proc. Natl. Acad. Sci. U.S.A. 103*, 2611–2616.
11. Lewis-Ballester, A., Batabyal, D., Egawa, T., Lu, C., Lin, Y., Marti, M. A., Capece, L., Estrin, D. A., and Yeh, S. R. (2009) Evidence for a ferryl intermediate in heme-based dioxygenases: Mechanistic implications. *Proc. Natl. Acad. Sci. U.S.A. 106*, 17371–17376.
12. Taniguchi, T., Sono, M., Hirata, F., Hayaishi, O., Tamura, M., Hayashi, K., Iizuka, T., and Ishimura, Y. (1979) Indoleamine 2,3-dioxygenase. Kinetic studies on the binding of superoxide anion and molecular oxygen to enzyme. *J. Biol. Chem. 254*, 3288–3294.
13. Ishimura, Y., Nozaki, M., and Hayaishi, O. (1970) The oxygenated form of L-tryptophan 2,3-dioxygenase as reaction intermediate. *J. Biol. Chem. 245*, 3593–3602.
14. Sono, M., Roach, M. P., Coulter, E. D., and Dawson, J. H. (1996) Heme-Containing Oxygenases. *Chem. Rev. 96*, 2841–2888.
15. Hirata, F., Ohnishi, T., and Hayaishi, O. (1977) Indoleamine 2,3-dioxygenase. Characterization and properties of enzyme·O_2^- complex. *J. Biol. Chem. 252*, 4637–4642.
16. Sono, M., Taniguchi, T., Watanabe, Y., and Hayaishi, O. (1980) Indoleamine 2,3-dioxygenase. Equilibrium studies of the tryptophan binding to the ferric, ferrous, and CO-bound enzymes. *J. Biol. Chem. 255*, 1339–1345.
17. Lu, C., Lin, Y., and Yeh, S. R. (2009) Inhibitory substrate binding site of human indoleamine 2,3-dioxygenase. *J. Am. Chem. Soc. 131*, 12866–12877.

18. Papadopoulou, N. D., Mewies, M., McLean, K. J., Seward, H. E., Svistunenko, D. A., Munro, A. W., and Raven, E. L. (2005) Redox and Spectroscopic Properties of Human Indoleamine 2,3-Dioxygenase and A His303Ala Variant: Implications for Catalysis. *Biochemistry 44*, 14318–14328.
19. Nickel, E., Nienhaus, K., Lu, C., Yeh, S. R., and Nienhaus, G. U. (2009) Ligand and substrate migration in human indoleamine 2,3-dioxygenase. *J. Biol. Chem. 284*, 31548–31554.
20. Terentis, A. C., Thomas, S. R., Takikawa, O., Littlejohn, T. K., Truscott, R. J., Armstrong, R. S., Yeh, S. R., and Stocker, R. (2002) The heme environment of recombinant human indoleamine 2,3-dioxygenase. Structural properties and substrate-ligand interactions. *J. Biol. Chem. 277*, 15788–15794.
21. Sohl, C. D., Isin, E. M., Eoff, R. L., Marsch, G. A., Stec, D. F., and Guengerich, F. P. (2008) Cooperativity in oxidation reactions catalyzed by cytochrome P450 1A2: Highly cooperative pyrene hydroxylation and multiphasic kinetics of ligand binding. *J. Biol. Chem. 283*, 7293–7308.
22. Lu, C., Mukai, M., Lin, Y., Wu, G., Poole, R. K., and Yeh, S. R. (2007) Structural and functional properties of a single domain hemoglobin from the food-borne pathogen *Campylobactor jejuni*. *J. Biol. Chem. 282*, 25917–25928.
23. Chauhan, N., Basran, J., Efimov, I., Svistunenko, D. A., Seward, H. E., Moody, P. C., and Raven, E. L. (2008) The role of serine 167 in human indoleamine 2,3-dioxygenase: A comparison with tryptophan 2,3-dioxygenase. *Biochemistry 47*, 4761–4769.
24. Denisov, I. G., Makris, T. M., Sligar, S. G., and Schlichting, I. (2005) Structure and chemistry of cytochrome P450. *Chem. Rev. 105*, 2253–2277.
25. Rousseau, D. L., Li, D., Couture, M., and Yeh, S. R. (2005) Ligand-protein interactions in nitric oxide synthase. *J. Inorg. Biochem. 99*, 306–323.
26. Das, A., Grinkova, Y. V., and Sligar, S. G. (2007) Redox potential control by drug binding to cytochrome P450 3A4. *J. Am. Chem. Soc. 129*, 13778–13779.
27. Presta, A., Weber-Main, A. M., Stankovich, M. T., and Stuehr, D. J. (1998) Comparative effects of substrates and pterin cofactor on the heme midpoint potential in inducible and neuronal nitric oxide synthases. *J. Am. Chem. Soc. 120*, 9460–9465.
28. Terness, P., Kallikourdis, M., Betz, A. G., Rabinovich, G. A., Saito, S., and Clark, D. A. (2007) Tolerance signaling molecules and pregnancy: IDO, galectins, and the renaissance of regulatory T cells. *Am. J. Reprod. Immunol. 58*, 238–254.
29. Torres, M. I., Lopez-Casado, M. A., Lorite, P., and Rios, A. (2007) Tryptophan metabolism and indoleamine 2,3-dioxygenase expression in coeliac disease. *Clin. Exp. Immunol. 148*, 419–424.
30. Bunn, H. F., and Poyton, R. O. (1996) Oxygen sensing and molecular adaptation to hypoxia. *Physiol. Rev. 76*, 839–885.
31. McCormick, C. C., Li, W. P., and Calero, M. (2000) Oxygen tension limits nitric oxide synthesis by activated macrophages. *Biochem. J. 350*, 709–716.
32. Kim, D., Heo, Y. S., and Ortiz de Montellano, P. R. (2008) Efficient catalytic turnover of cytochrome P450(cam) is supported by a T252N mutation. *Arch. Biochem. Biophys. 474*, 150–156.
33. Forouhar, F., Anderson, J. L., Mowat, C. G., Vorobiev, S. M., Hussain, A., Abashidze, M., Bruckmann, C., Thackray, S. J., Seetharaman, J., Tucker, T., Xiao, R., Ma, L. C., Zhao, L., Acton, T. B., Montelione, G. T., Chapman, S. K., and Tong, L. (2007) Molecular insights into substrate recognition and catalysis by tryptophan 2,3-dioxygenase. *Proc. Natl. Acad. Sci. U.S.A. 104*, 473–478.
34. Uchida, K., Shimizu, T., Makino, R., Sakaguchi, K., Iizuka, T., Ishimura, Y., Nozawa, T., and Hatano, M. (1983) Magnetic and natural circular dichroism of L-tryptophan 2,3-dioxygenases and indoleamine 2,3-dioxygenase. II. Spectra of their ferric cyanide and ferrous carbon monoxide complexes and an oxygenated form. *J. Biol. Chem. 258*, 2526–2533.
35. Sono, M. (1990) Spectroscopic and equilibrium studies of ligand and organic substrate binding to indolamine 2,3-dioxygenase. *Biochemistry 29*, 1451–1460.